Alternative analytical models for HTS tapes considering their AC hysteretic and resistive losses

Alternative Analytical Models for HTS Tapes Considering their AC Hysteretic and Resistive Losses

João F. P. Fernandes[1*], Luís F. D. Bucho[1], F. Ferreira da Silva[1], Inês S. P. Peixoto[2], Silvio Vaschetto[2] and P. J. Costa Branco[1]

[1] IDMEC, Instituto Superior Técnico, Universidade de Lisboa, Lisbon, Portugal
[2] Dipartimento Energia "G. Ferraris", Politecnico di Torino, Torino, Italy

*E-mail: joao.f.p.fernandes@tecnico.ulisboa.pt

Received xxxxxx
Accepted for publication xxxxxx
Published xxxxxx

Abstract

This work proposes two alternative analytical models to evaluate the *ac* losses of High-Temperature Superconducting (HTS) tapes during their hysteretic and resistive modes. These models intend to extend the application range of state-of-the-art analytical models for current values higher than the critical one, i.e., for the resistive state, and to correctly predict the *ac* losses during the transition between the hysteretic and resistive modes. Two analytical models are proposed, one considering an extension of the Norris model for the HTS tape's resistive mode and the other based on a Sigmoid function to characterize the hysteretic losses and their smooth transition to the resistive mode. Analytical models capable of estimating *ac* losses of superconducting (SC) tapes are an important tool for the design of complex SC systems, such as SC fault current limiters, SC electrical machines and SC cables. The proposed models are validated experimentally, for a 1st generation BSCCO tape and a 2nd generation ReBCO tape. Finite element simulation is also carried out to verify the accuracy of the proposed models. Results show that the proposed Extended-Norris model presents some deviation at the transition between the hysteretic and resistive modes, while the Sigmoid model presents very accurate results for the whole spectrum of applied current. Also, the parameters of the Sigmoid models are independent of the tape geometry.

Keywords: Analytical model, Equivalent circuit; Hysteretic losses, Resistive losses, HTS Tape, Experimental tests, BSCCO, ReBCO.

1. Introduction

The use of High-Temperature Superconductors (HTS) in electrical machines has been identified as a potential technology to unlock the further electrification of transportation systems [1]-[2], specifically in aeronautical transportation [3]-[7]. Using HTS materials, such as bulks and tapes, fully [3] and partial [5] superconducting electric machines are being designed with different topologies, such as radial and axial flux synchronous machines and superconducting induction machines [6]-[8].

With the continuous developments of HTS technologies, the existing limitations of superconductors are being surpassed [9]. While some limitations still remain, the current HTS materials already offer some key advantages due to their facilitated

cooling, their high critical current, and near-zero DC losses. However, under *ac* conditions, HTS materials, such as tapes or bulks, present non-negligible losses that must be considered in the design of electrical components [10]. It is imperative to estimate their *ac* losses during the design stage of electrical devices because they affect their efficiency and the operation of the superconductors (SC).

The *ac* losses computation can be performed through the use of Finite Element Analysis tools (FEA), using multiple electromagnetic formulations, such as *H*-, *H-A,* or *T-A* formulations [11]-[13], or using approximated analytical equations [14]-[15]. While FEA tools present an accurate method to estimate the SC losses, they require high computational times. Hence, they may not be compatible with early design stages of electromechanical devices, where the basic topology is still to be determined. Analytical models, such as the Norris model [14], offer advantages for early design stages due to their easy computation, physical interpretation, and sufficiently accurate results under some assumptions. These analytical models were already presented in the literature for HTS bulks and tapes.

In [14], Norris presents an analytical model for *ac* losses in elliptical and thin-strips HTS tapes under the assumption of constant critical current, i.e., independent of the magnetic field. While this assumption seems limited, studies show that the model is a good approximation to experimental results, when the critical current is not surpassed [16]-[17]. In [15], Ernst Brandt proposed analytical models for the thin strip under a) an applied current, b) an applied perpendicular magnetic field, and c) both applied current and perpendicular magnetic field. This model was further developed in [18] and verified against experimental results [19]-[20].

While still limited in their applications, these analytical models already present important advantages for the early design stages of electrical devices. However, some applications still require more complete models, where the transitions between the SC hysteresis and resistive losses are important. Some examples are:

- In the design optimization and transient analysis of short-circuits in HTS cables, for power transmission. These are typically characterized by a high number of tapes in parallel and working conditions that include the transition between the hysteretic and resistive models [21]-[23];
- In the supervision and analysis of transient performance of superconducting fault current limiters (SFCL) [24]-[27];
- In HTS induction machines where the SC exceeds its critical current during its start-up conditions and reaches its hysteretic state near synchronism [28]-[29], and;
- In the identification of HTS tapes parameters under experimental *ac* tests [30]-[32].

Following this research line, these models can be corrected and extended to cover a wider range of operating conditions. This work focuses on improving these analytical models for the computation of *ac* losses in a wider range of operations. More specifically, the novelty of this work resides in a) the extension of their use for current values higher than the critical current (resistive losses), b) the correction of their behaviour when approaching the critical current (transition between the hysteretic and resistive models), and c) when in the presence of magnetic fields (self *ac* and external *dc*). Besides the improvements proposed for the Norris and Brandt analytical models, a Sigmoid model is also proposed to better characterize the transition between the hysteretic and resistive losses of HTS tapes. For both modified Norris, Brandt and Sigmoid models, lumped parameters models are also developed, and experimental results are shown to validate their applicability.

This work is divided into 5 sections. In the first section, the introduction, novelty, and relevance of this work are highlighted. In section 2, the proposed analytical models are presented. Experimental methodology and results are presented in sections 3 and 4. The discussion and conclusions are made in sections 5 and 6.

2. Extended Norris Analytical Formulation

The Norris model is only valid for $I_m<I_c$, where I_m is the amplitude of the applied current and I_c is the critical current amplitude. Thus, this model is not valid for the resistive behaviour of the HTS tape, i.e., for $I_m>I_c$, and does not consider the impact of the average magnetic flux density (self *ac* and external *dc*) on the critical current. To overcome these limitations two analytical models are proposed: an "extended Norris model" and a "Sigmoid Model".

a) Extended Norris Model: based on the Norris model [14] for the hysteretic behaviour of the *ac* HTS tape for $I_m<I_c$, and the resistive losses based on the E-J power law;
b) Sigmoid Model: based on a Sigmoid function to represent the hysteretic losses for all values of currents and the resistive losses based on the E-J power law.

Due to the characteristics of the proposed extended Norris model, the hysteretic losses in the Norris model are only defined for $I_m < I_c$, making the model defined by parts. This creates the illusion of a "knee" point on the losses evolution, as a function of the current, in the transition between the hysteretic and resistive zones. To avoid this discontinuity effect, a Sigmoid function is proposed to characterize the hysteretic losses, introducing a smoother transition between the hysteretic and resistive modes. Within this framework, this analytical model presents a unique and continuous function for all ranges of current amplitudes.

2.1. Extended-Norris Analytical Model

The losses on the superconductor can be estimated considering two different amplitudes for the current: $I_m < I_c$ and $I_m \geq I_c$. In this model, it is considered that hysteretic losses occur when $I_m < I_c$, and both hysteretic and normal resistive losses occur when $I_m \geq I_c$. Disregarding the magnetization initial

losses, the steady-state losses are computed considering a sinusoidal current is applied to the tape, $I(t)=I_m\cos(\omega t)$. The Extended-Norris model is thus developed for typical 1st generation elliptical HTS tapes and for 2nd generation thin strips HTS tapes.

2.1.1.Hysteretic Stage ($I_m < I_c$)

For $I_m < I_c$, the hysteretic losses can be computed considering the same approach proposed by Norris by computing half of the losses from I_m to $-I_m$, where the reverse supercurrents penetrate the superconductor. In detail, Norris computed the losses, L_c, in elliptical and thin-strip superconductors as in (1) and (2), respectively [14].

$$L_{c\_ellipse} = \frac{\mu_0 I_c^{\,2}}{\pi}\left((1-F)\ln(1-F)+(2-F)\frac{F}{2}\right) \quad (1)$$

$$L_{c\_thin} = \frac{\mu_0 I_c^{\,2}}{\pi}\left((1-F)\ln(1-F)+(1+F)\ln(1+F)-F^2\right) \quad (2)$$

I_c is the critical current amplitude and $F = I_m/I_c$. The average value of the hysteretic losses, P_{hyst}, can be computed considering the applied electric frequency, f:

$$P_{hyst\_ellipse} = \frac{f\mu_0 I_c^{\,2}}{\pi}\left((1-F)\ln(1-F)+(2-F)\frac{F}{2}\right) \quad (3)$$

$$P_{hyst\_thin} = \frac{f\mu_0 I_c^{\,2}}{\pi}\left((1-F)\ln(1-F)+(1+F)\ln(1+F)-F^2\right) \quad (4)$$

2.1.2.Resistive and Hysteretic Stages ($I_m > I_c$)

When the current amplitude is higher than the critical current, $I_m > I_c$, it is assumed that the hysteretic losses still occur instantaneously when $I(t) < I_c$, i.e., while the current is lower than the critical current. This means the hysteretic losses remain equal to their maximum value for any current amplitude higher than the critical current ($F\rightarrow 1$). The maximum value of the hysteretic losses can be defined by computing the limit of (1) and (2) when $F\rightarrow 1$, as reported in (5) and (6).

$$F \rightarrow 1 \Rightarrow P_{hyst\_ellipse} = \frac{1}{2}\frac{f\mu_0 I_c^{\,2}}{\pi} \quad (5)$$

$$F \rightarrow 1 \Rightarrow P_{hyst\_thin} = \frac{f\mu_0 I_c^{\,2}}{\pi}(\ln(4)-1) \quad (6)$$

Instantaneously, when $I(t) \geq I_c$, the power law is used to estimate the resistive losses. This can be done using the E-J power law in (7), where E_c is the critical electric field that defines the critical current density, J_c, and n is the power-law coefficient. The resistive losses can be determined by computing the average value of the resistive losses, assuming a uniform distribution of the current density in the HTS tape and $I(t) = I_m\cos(\omega t)$, (8). Using a variable transformation, $\theta = \omega t$, and the integral of a power cosine in (9), the final expression for the resistive losses, P_{resist}, can be achieved in (10), for both the elliptical and thin-strip HTS tapes.

$$E = \rho(J)J = E_c\left|\frac{J}{J_c}\right|^n \quad (7)$$

$$P_{resist} = \frac{1}{T}\int_0^T E\cdot I(t)dt = \frac{1}{T}\int_0^T \frac{E_c}{I_c^{\,n}}\cdot I(t)^{n+1}dt = \\ = \frac{1}{2\pi}\frac{E_c}{I_c^{\,n}} I_m^{\,n+1}\int_0^{2\pi}\cos(\theta)^{n+1}d\theta \quad (8)$$

$$\int_0^{2\pi}\cos^{n+1}(\theta)d\theta = \frac{\pi}{2^n}\frac{(n+1)!}{\left(\frac{n+1}{2}!\right)^2} \quad (9)$$

$$P_{resist} = \frac{E_c}{2^{n+1}}\frac{I_m^{\,n+1}}{I_c^{\,n}}\frac{(n+1)!}{\left(\frac{n+1}{2}!\right)^2} = \frac{F^{n+1}I_cE_c}{2^{n+1}}\frac{(n+1)!}{\left(\frac{n+1}{2}!\right)^2} \quad (10)$$

Therefore, the total superconducting tape losses when $I_m \geq I_c$ can be obtained using (11) and (12), considering the hysteretic and resistive losses.

$$P_{ellipse} = \frac{1}{2}\frac{f\mu_0 I_c^{\,2}}{\pi} + \frac{F^{n+1}I_cE_c}{2^{n+1}}\frac{(n+1)!}{\left(\frac{n+1}{2}!\right)^2} \quad (11)$$

$$P_{thin} = \frac{f\mu_0 I_c^{\,2}}{\pi}(\ln(4)-1) + \frac{F^{n+1}I_cE_c}{2^{n+1}}\frac{(n+1)!}{\left(\frac{n+1}{2}!\right)^2} \quad (12)$$

Note that when parameter n is high, which is the typical case of HTS, the expression for the resistive losses in (10) can also be used for $I_m < I_c$ because, for this range of current amplitude, the resistive losses are typically much lower than the hysteretic losses. Thus, for the whole range of current amplitude, the HTS losses can be approximated by (13) and (14).

$$P_{ellipse} = \frac{f\mu_0 I_c^{\,2}}{\pi}\left((1-\Gamma)\ln(1-\Gamma)+(2-\Gamma)\frac{\Gamma}{2}\right)+ \\ + \frac{F^{n+1}I_cE_c}{2^{n+1}}\frac{(n+1)!}{\left(\frac{n+1}{2}!\right)^2}, \quad \Gamma = \min(F,1) \quad (13)$$

$$P_{thin} = \frac{f\mu_0 I_c^{\,2}}{\pi}\left((1-\Gamma)\ln(1-\Gamma)+(1+\Gamma)\ln(1+\Gamma)-\Gamma^2\right)+ \\ + \frac{F^{n+1}I_cE_c}{2^{n+1}}\frac{(n+1)!}{\left(\frac{n+1}{2}!\right)^2}, \quad \Gamma = \min(F,1) \quad (14)$$

An example of the Extended-Norris analytical model's losses is shown in Fig. 1 for an elliptical superconductor with $I_c = 140$ A and $n = 11$. Results from a Finite Element Analysis

(FEA) tool are also present in this figure, for the same elliptical superconductor, considering a magnetic field independent critical current (Bean model [33]) and an *H*-formulation. More details about the FEA model are presented in the next sections. For the Extended-Norris analytical model, the zones where the hysteretic losses are predominant, $I_m < I_c$, and where the resistive losses are predominant, $I_m \geq I_c$ are easily verifiable. A "knee" point separates the two zones, due to the rapid limitation of the hysteretic analytical losses, as seen in Fig. 1 at $I_m = I_c$. To avoid this, the Sigmoid model is presented in section 2.2.

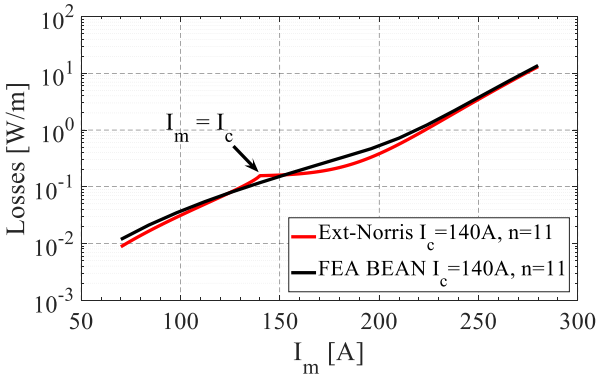

Fig. 1. Illustration HTS tape losses for I_c = 140 A and n = 11, considering Extended-Norris and the FEA BEAN model results.

2.2. Sigmoid Analytical Model

The merit of the Sigmoid function is to be capable of representing the hysteretic losses and introducing a continuous transition to the resistive mode. The hysteretic and resistive losses from the Extended-Norris model are represented in Fig. 2(a) for an elliptical superconductor with I_c = 140 A and n = 11. While the resistive losses present a continuous behaviour, the hysteretic losses stop increasing drastically at $F = 1$, thus creating the "knee" point shown in Fig. 1. A Sigmoid function, (15), was tested to replace the hysteretic losses defined by Norris, to assure a smooth transient to the resistive state. In Fig. 2(b) is shown a comparison between the hysteretic Norris model and a Sigmoid function.

As a result, when using a Sigmoid function to replace the Norris hysteretic losses, there is a smooth transition between the hysteretic and resistive zones, and also a single continuous function to describe the whole range of current P_{losses}, (16).

$$P_{hyst\_ellipse} = \frac{f\mu_0 I_c^{\,2}}{\pi} sigmoid(F-1)$$

$$P_{hyst\_ellipse} = \frac{f\mu_0 I_c^{\,2}}{\pi}\left(\frac{a}{\left(1+\exp\left(-b\left(F-1\right)\right)\right)^c}\right) \quad (15)$$

$$P_{losses} = \frac{f\mu_0 I_c^{\,2}}{\pi}\left(\frac{a}{\left(1+\exp\left(-b\left(F-1\right)\right)\right)^c}\right) + \frac{F^{n+1} I_c E_c}{2^{n+1}} \frac{(n+1)!}{\left(\frac{n+1}{2}!\right)^2} \quad (16)$$

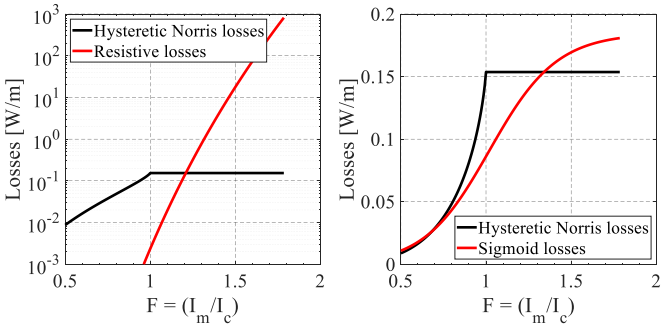

Fig. 2. (a) Separation of losses using the Extended-Norris model with a logarithmic *y*-axis, and (b) comparison between the Norris hysteretic model and a Sigmoid function.

Of course, parameters *a*, *b* and *c* of the Sigmoid functions need to be calibrated for elliptical and thin-strip tapes. The best results for elliptical and thin-film HTS tapes were obtained for a = 0.8 and b = 5 for both tapes and c = 1.25 for the elliptical and c = 1.5 for the thin-strip tapes. In Fig. 3 are shown the analytical results for the Extended-Norris and Sigmoid model losses and the FEA Bean model, for an elliptical tape with I_c = 140 A and n = 11.

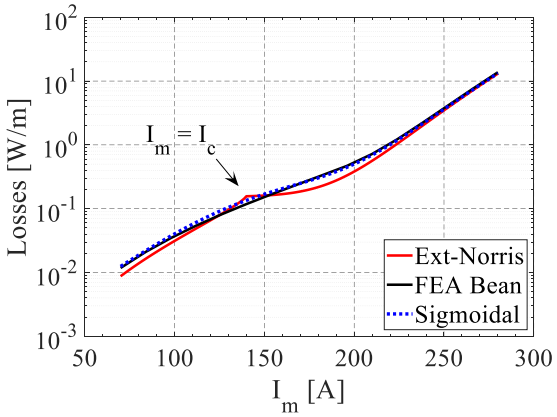

Fig. 3. Comparison between the Extended-Norris and Sigmoid models with a=0.8, b=5 and c=1.25. I_c = 140 A, n = 11.

To evaluate the influence of each parameter of the Sigmoid function in the full losses curve, a sensitivity analysis applying a change of ±20% for *a*, *b*, and *c* coefficients was conducted. Results are presented in Fig. 4 to Fig. 6 for a change in parameters *a*, *b* and *c,* respectively. Parameter *a* introduces an offset on the *ac* hysteretic losses (I_m<140A), while *b* and *c* introduce a different slope in this zone. The influence of parameter *b* is only visible for current values lower than 120A,

while parameter *c* introduces an influence for current values lower than 160A. To calibrate the proposed model, the following methodology can be used: both parameters *b* and *c* can be calibrated using the slope of the hysteretic losses, while parameter *a* can be calibrated to adjust its offset.

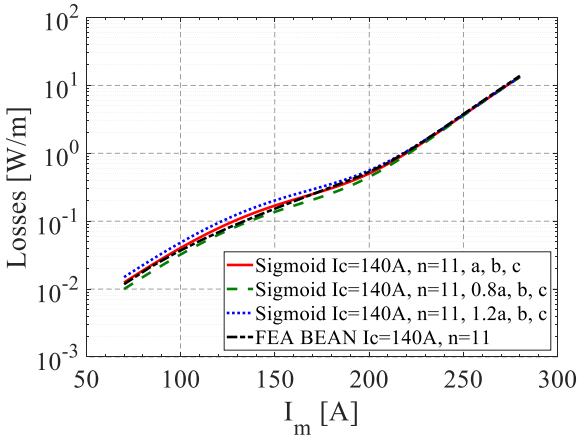

Fig. 4. Variation of parameter *a* in the Sigmoid model.

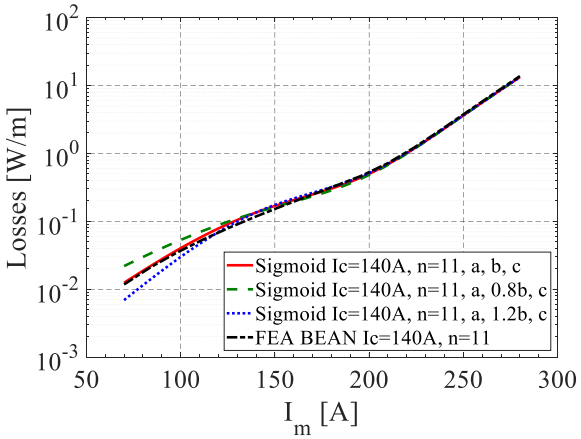

Fig. 5. Variation of parameter *b* in the Sigmoid model.

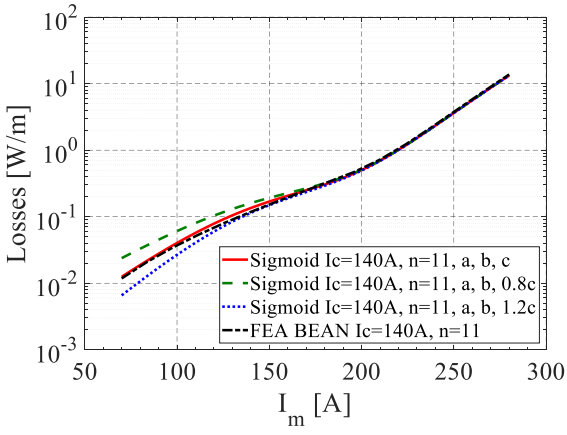

Fig. 6. Variation of parameter *c* in the Sigmoid model.

2.3. Influence of the Self-Magnetic Field

For elliptical superconductors, which are typically the 1st generation tapes, the incorporation of the change of the critical current density with the SC self-magnetic field produces an analytical solution without closed-form. However, it has been verified that considering an average value of the self-magnetic field results in a better estimation of the HTS parameters. This can be done in an iterative process shown in Fig. 7, where I_{c0} is the critical current density at no magnetic field, B_{av} is the average value of the superconductor magnetic flux density, and B_0 is the value of magnetic flux density that reduces the critical current density to half.

$$I_m \rightarrow F = \frac{I_m}{I_c} \rightarrow B_{av}(F) \rightarrow I_c(B_{av}) = \frac{I_{c0} B_0}{B_0 + B_{av}}$$

Fig. 7. Iterative process for the inclusion of the average magnetic field.

For the 2nd generation thin-strip superconductors Brandt already calculated the flux through half of a strip as a function of *F*, for $I_m < I_c$, (17) [15]. With this, the average magnetic flux density can be computed, $B_{av}(F)$, (18), where *a* is half of the superconducting tape width and h_{tape} is its height, Fig. 8.

$$\phi_h = \frac{\mu_0 J_c h_{tape} a}{2\pi}\left[(1+\Gamma)\ln(1+\Gamma)+(1-\Gamma)\ln(1-\Gamma)\right], \quad \Gamma = \min(F,1) \tag{17}$$

$$B_{av} = \frac{1}{a}\int_0^a B(x)\,dx = \frac{1}{a}\phi_h \tag{18}$$

When the full penetration of the currents is achieved ($F \geq 1$), the distribution of the magnetic flux density is assumed constant, but its amplitude increases with $F = I_m/I_c$. This can be added by multiplying it with a max(.) function as described in (19).

$$B_{av} = \frac{\mu_0 J_c h_{tape}}{2\pi}\left[(1+\Gamma)\ln(1+\Gamma)+(1-\Gamma)\ln(1-\Gamma)\right]\cdot\max(F,1) \tag{19}$$

For the elliptical tapes, Norris avoided computing the average value of the magnetic flux density to compute the superconducting losses [14]. However, this value can be estimated using Ampère's law and assuming elliptical contours of the magnetic field, *H*. Of course, assuming elliptical contours of *H* leads to an unfeasible solution due to the conservation of magnetic flux. Nevertheless, this unfeasible solution is a good approximation for the magnetic field average value along the tape. Considering Ampère's law in (20), the evolution of the magnetic field, for $I_m < I_c$, can be estimated, where $k = b/a$, *a* and *b* are the ellipse semi-major and semi-minor axis, and x_0 corresponds to the penetration of the supercurrents, Fig. 8. The term $P(x)$ is the perimeter of the ellipse with a major axis *x*. This perimeter does not have an analytical solution but can be estimated using the approximation (21) [34].

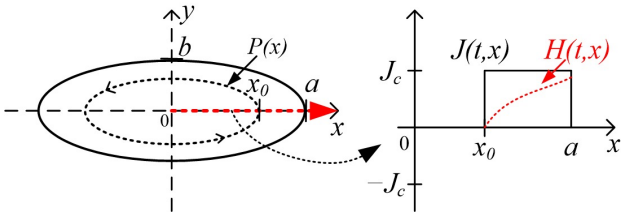

Fig. 8. Elliptical wire geometry and penetration of the magnetic field.

$$\oint \mathbf{H}d\mathbf{l} = \iint_{S(x)} \mathbf{J}\mathbf{n}ds \Leftrightarrow$$

$$\Leftrightarrow P(x)H(x) = \begin{cases} 0, & x < x_0 \\ J_c \pi k (x^2 - x_0^2), & x_0 < x < a \end{cases} \tag{20}$$

$$P(x) \cong \pi x \sqrt{2(1+k^2)} \tag{21}$$

The magnetic field and the average value of the magnetic flux density can be obtained from (22) to (23).

$$H_{sc}(x) = \begin{cases} 0, & x < x_0 \\ \dfrac{J_c k \left(x^2 - x_0^2\right)}{x\sqrt{2\left(1+k^2\right)}}, & x_0 \le x \le a \end{cases} \tag{22}$$

$$B_{av} = \frac{1}{a}\int_0^a \mu_0 H(x)\,dx = \frac{1}{a}\int_{x0}^a \mu_0 \frac{J_c k\left(x^2 - x_0^2\right)}{x\sqrt{2\left(1+k^2\right)}}\,dx =$$

$$= \frac{\mu_0 J_c k a}{2\sqrt{2\left(1+k^2\right)}}\left[\Gamma + (1-\Gamma)\ln(1-\Gamma)\right], \tag{23}$$

$$\Gamma = \min(F,1), \quad F = \frac{I_m}{I_c} = 1 - \frac{x_0^2}{a^2}$$

Similar to the thin-strip HTS tape, when the full penetration is achieved, the distribution of the magnetic flux density is assumed constant, however, its amplitude increases with F. Therefore, its average value can be described as shown in (24).

$$B_{av} = \frac{\mu_0 J_c k a}{2\sqrt{2\left(1+k^2\right)}}\left[\Gamma + (1-\Gamma)\ln(1-\Gamma)\right]\cdot \max(F,1) \tag{24}$$

2.4. Equivalent resistance

From these analytical models, equivalent HTS tape resistances per unit length can be determined for a sinusoidal applied current. Considering $I_m = \sqrt{2} I_{rms}$, the equivalent HTS tape resistance per meter can be defined as in (25) and (26), for the elliptical and thin-strip HTS tapes, respectively. The HTS tape's losses can be computed using $P_{total} = R_{eq} I_{rms}^2$, dividing equations (13), (14) and (16) by I_{rms}^2.

Using the Extended-Norris model, for 1st generation elliptical superconductors:

$$R_{eq} = R_{eq_{hyst}} + R_{eq_{resist}} = \\ = \frac{2 f \mu_0}{\pi F^2}\left((1-\Gamma)\ln(1-\Gamma) + (2-\Gamma)\frac{\Gamma}{2}\right) + \\ + \frac{F^{n-1} E_c}{2^n I_c}\frac{(n+1)!}{\left(\frac{n+1}{2}!\right)^2}, \quad \Gamma = \min(F,1) \tag{25}$$

Using the Extended-Norris model for 2nd generation thin-strip superconductors:

$$R_{eq} = R_{eq_{hyst}} + R_{eq_{resist}} = \\ = \frac{2 f \mu_0}{\pi F^2}\left((1-\Gamma)\ln(1-\Gamma) + (1+\Gamma)\ln(1+\Gamma) - \Gamma^2\right) + \\ + \frac{F^{n-1} E_c}{2^n I_c}\frac{(n+1)!}{\left(\frac{n+1}{2}!\right)^2}, \quad \Gamma = \min(F,1) \tag{26}$$

Using the Sigmoid model for both 1st and 2nd generation superconductors:

$$R_{eq} = R_{eq_{hyst}} + R_{eq_{resist}} = \\ = \frac{2 f \mu_0}{\pi F^2}\left(\frac{a}{\left(1+\exp\left(-b\left(F-1\right)\right)\right)^c}\right) + \\ + \frac{F^{n-1} E_c}{2^n I_c}\frac{(n+1)!}{\left(\frac{n+1}{2}!\right)^2}, \quad \Gamma = \min(F,1) \tag{27}$$

Note that F, Γ and I_c must be updated with the average values of the magnetic flux density, as described in section 2.3, Fig. 7.

3. Validation Methodology

Experimental tests are carried out with a 1st generation and a 2nd generation SC tape to validate the developed analytical models and verify their applicability. During these tests, a sinusoidal current is applied to the tape, the voltage is measured, and the losses are computed.

First, using the developed analytical models, the values I_c, B_0 and n are inferred from the experimental results, and then a FEA tool is used to validate the analytical models. As will be seen, this procedure is very useful and allows for the calibration of the HTS parameters from *ac* experimental results with the minimum computational requirements. One example is

provided in a spreadsheet file[1] with the equations for the analytical models and the presented experimental results. By optimizing the HTS tape's parameters in the analytical models, the designer can identify the most adequate range of parameters of the HTS tape. The superconducting tapes used are BSCCO and ReBCO tapes, whose geometric and characteristic parameters are shown in TABLE 1. Manufacturers provide a range of critical current, I_c, and n at DC conditions and self-field, due to their anisotropy along its length, however no information is provided regarding B_0. The latter was estimated based on literature [35]-[36]. The BSCCO tape was supplied by Nexans in 2008 (model C01-207) and the ReBCO tape was acquired from SuperPower in 2022 (model SCS4050-AP). The silver matrix of the BSCCO tape presents a non-linear electric resistivity with the temperature, however, for 77K its typical value is around $0.4\times 10^{-8}\Omega$m, slightly influenced by the Mg content [37]-[38].

TABLE 1
HTS 1ST GEN. BSCCO AND REBCO TAPES' CHARACTERISTICS

Characteristic	BSCCO (1st gen.)	ReBCO (2nd gen.)
I_c (77K) @ dc	160-180A	155-175A
n (77K) @ dc	10-13	30-35
B_0(77K) @ dc	0.1 - 0.14 T	0.1 - 0.14 T
Geometry	Elliptical	Thin strip
w_{sc} (w_{sc} = 2a)	3.5 mm	4.01 mm
h_{sc} (h_{sc} = 2b)	0.12 mm	0.095 mm
k = b/a	0.0343	-
Manufacturer	Nexans SuperConductors BSCCO-2212 C01-207	SuperPower SCS4050-AP

The experimental setup used consists of a sinusoidal voltage source, Keysight AC6804B, connected to a step-down transformer with the secondary connected to the HTS tapes. A cancelation coil is used to allow the alignment of the tape's voltage and current to reduce the error when computing the active power (losses). The voltage is measured using a micro-voltmeter, Keithley 2000, acquiring the voltage time evolution for at least 20 periods with around 40 points per period. Each measurement is repeated 5 times to mitigate noise. A schematic and photo of the experimental setup are shown in Fig. 9 and Fig. 10.

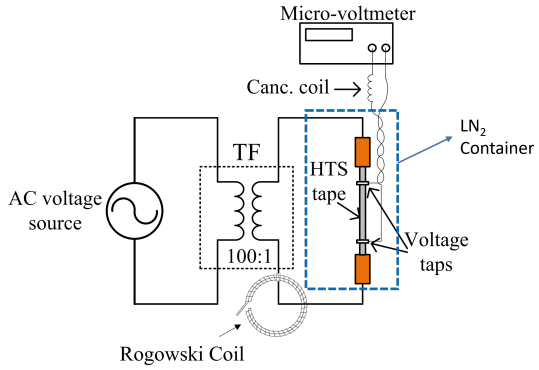

Fig. 9. Schematic of the experimental setup.

[1] File submitted as supplementary data. Will be published in database.

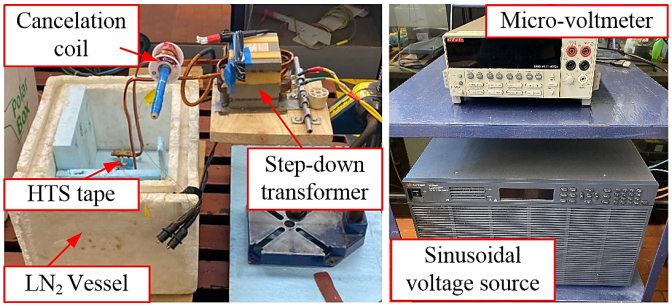

Fig. 10. Photo of the experimental setup.

4. Experimental and Simulation Results

In this section, the applicability and accuracy of the proposed analytical models are verified. First, the values of I_c, B_0 and n are calibrated, in the analytical models, to replicate the experimental results. Please note that the experimental results are done in *ac* conditions, thus, the simple definition of the critical current density, J_c, for E=E_c, is not valid. The manufacturers provide a range of critical current, J_c, and n at self-field. Using these values as a reference, the values of I_c, B_0 and n are adjusted to converge to the experimental *ac* results. Then, to verify the correctness of this method, using the analytically obtained HTS tape's parameters, FEM results are compared with the analytical and experimental ones. With the convergence between experimental, analytical and FEM results, the applicability of the proposed analytical models can be verified.

In Fig. 11 are presented the experimental losses per meter for both BSCOO and ReBCO tapes when applying sinusoidal currents with f = 50 Hz. The current amplitude was changed between 50 to 280 A for the BSCCO tape and between 50 to 190 A for the ReBCO tape. The latter presents lower losses than the BSCCO until the resistive state is reached. In the resistive state, the slope presented by the ReBCO is higher than the one presented by the BSCCO.

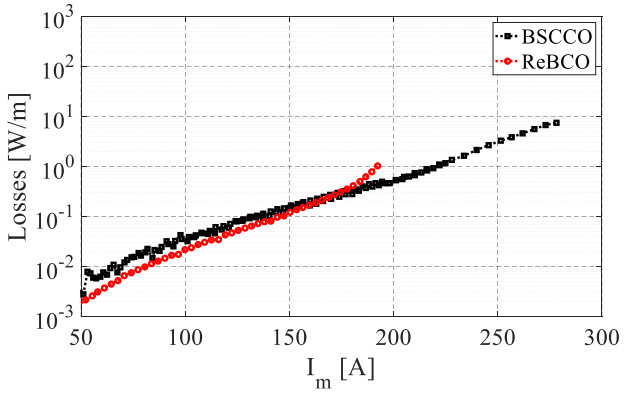

Fig. 11. Experimental results for the BSCCO and ReBCO tape.

4.1. Determination of the Tapes' I_c and n values

4.1.1. BSCCO Tape

In Fig. 12 to Fig. 15, the experimental results are compared with the analytical models, for different combinations of parameters I_{c0}, B_0 and n values. In particular, Fig. 12 and Fig. 13 present the results from the analytical Extended-Norris model, and Fig. 14 and Fig. 15 present the results from the Sigmoid model.

The parameter n can be calibrated by finding the value that reproduces a similar slope of the resistive losses, i.e., $I_m \geq I_c$, when compared with the experimental results. It has been found that, for the BSCCO tape, $n = 11$ reproduces the closest results for the resistive losses. The critical current, I_{c0}, and B_0 values can be determined by inspecting the hysteretic losses for values of current lower than the critical one, $I_m < I_c$. This is because these values influence the slope and offset of the hysteretic losses, as seen in Fig. 12 and Fig. 14 for the Extended-Norris and Sigmoid models, respectively. The values I_{c0} = 175 A, $B_0 = 0.14$ T and $n = 11$ result in the closest hysteretic and resistive losses to the experimental ones.

The developed analytical models helped identify the characteristic values of the BSCCO tape. Compared with the Extended-Norris model, the Sigmoid model has better results during the transition between the superconducting and resistive modes. Please note that the self-magnetic field of the tape is considered in the analytical models.

Additionally, the analytical models for very high values of currents start to deviate from the experimental results. This is due to the presence of the silver matrix in the 1st generation BSCCO tape, as explained in the next subsection.

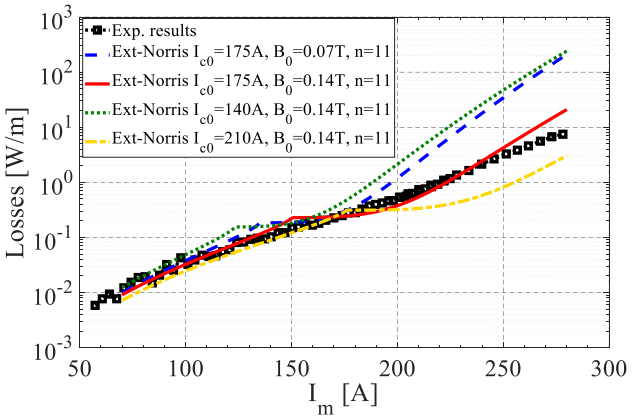

Fig. 12. BSCCO experimental and analytical Extended-Norris results for different critical currents, "I_{c0}" parameters.

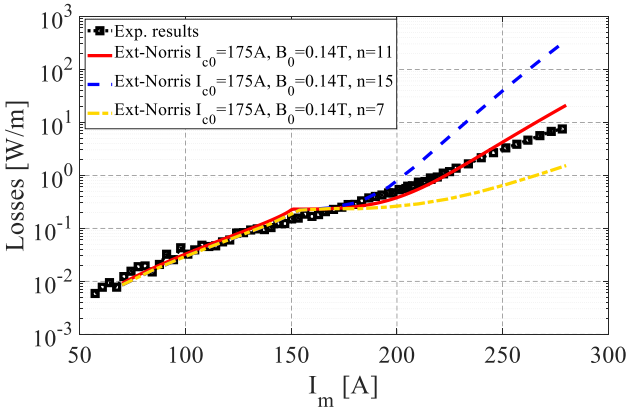

Fig. 13. BSCCO experimental and analytical Extented-Norris results for different "n" parameters.

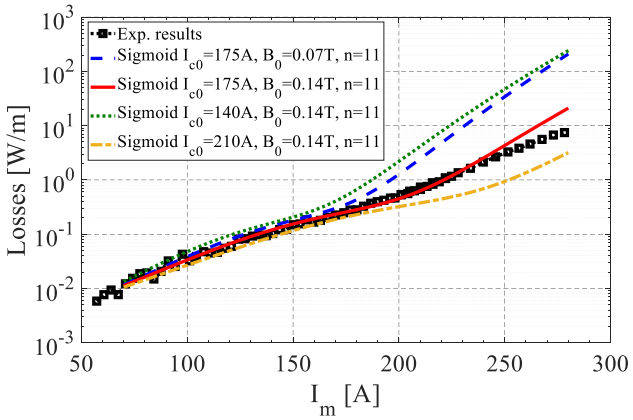

Fig. 14. BSCCO experimental results and analytical Sigmoid results for different "I_{c0}" parameters.

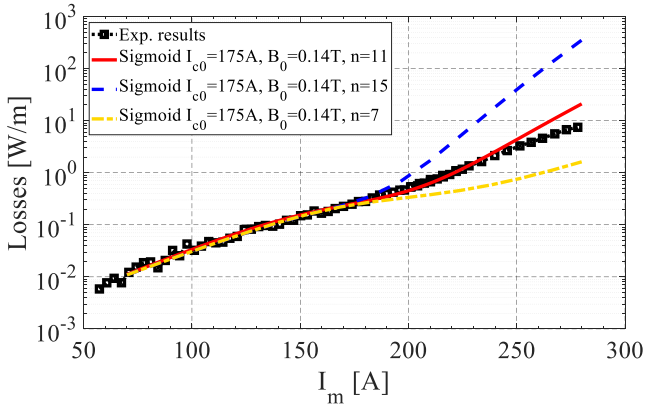

Fig. 15. BSCCO experimental and analytical Sigmoid results for different "n" parameters.

4.1.2. ReBCO Tape

In Fig. 16 and Fig. 17, the experimental results are compared with the analytical models, for different combinations of parameters I_{c0}, B_0 and n values. It can be seen that the Extended-Norris model diverges from the experimental results for lower

values of currents but presents good results for values of currents I_m>100 A, when I_{c0}=162 A, B_0=0.14 T and n=21. Thus, the resistive state is well defined while the Norris equation presents some deviations. This deviation was also verified in different works for ReBCO tapes [17], [20].

The sigmoid model presents accurate results for the whole range of applied current, with the same parameters I_{c0}=162 A, B_0=0.14 T and n=21. These parameters are coherent with the manufacturer data presented in TABLE 1.

To verify the accuracy of the analytical models and the identified parameters, each tape is simulated using a FEA tool. These results are shown in the following section.

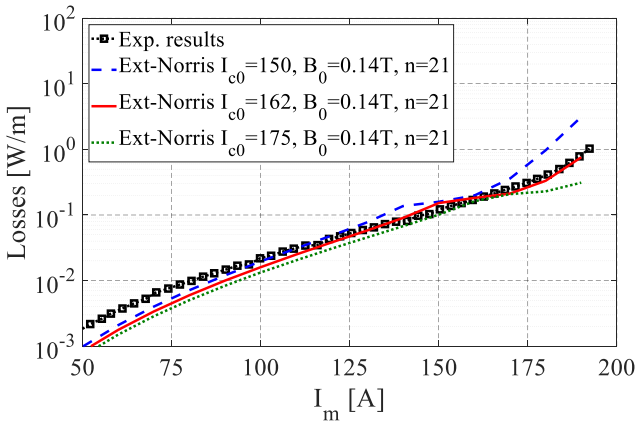

Fig. 16. ReBCO experimental results and analytical ext-Norris results for different critical currents "I_{c0}".

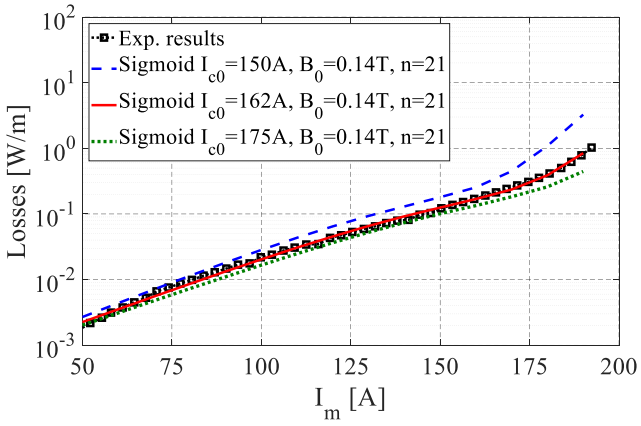

Fig. 17. ReBCO experimental and analytical Sigmoid results for different critical currents "I_{c0}".

4.2. Validation of the analytical model

FEA simulations are carried out to validate the analytical models using the H-formulation [39] to simulate the 1st generation elliptical tape and the T-formulation [40] to simulate the 2nd generation thin strip tape. For each tape, the Kim model together with the SC power law are used. The meshes used for both FEA simulations are shown in Fig. 18 and Fig. 19, with 2268 triangular elements for the BSCCO tape and 50 edge elements for the ReBCO tape. For the 1st generation BSCCO tape, in Fig. 18, firstly was considered an air layer around the BSCCO layer, and secondly the silver layer which is, in fact, around the BSCCO layer.

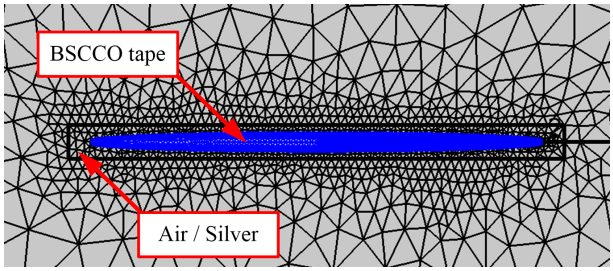

Fig. 18. FEA mesh used for the 1st Generation BSCCO.

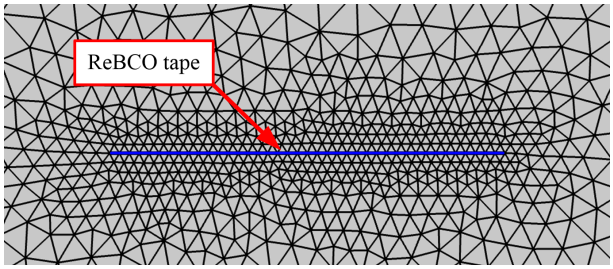

Fig. 19. FEA mesh used for the 2nd Generation ReBCO.

4.2.1.BSCCO Tape

The experimental, Extended-Norris, Sigmoid model and FEA results are shown in Fig. 20 and Fig. 21 for the BSCCO tape. In Fig. 20, no silver layer is considered around the SC layer, while in Fig. 21 the silver layer is considered. In both figures, the FEA results are close to the analytical ones, for the same input parameters of the HTS tape. It is possible to obtain similar results using the FEA Kim model, with I_{c0} = 175 A, B_0 = 0.14 T and n = 11. In Fig. 20, for values of current amplitudes higher than 250A, both analytical and simulation results start deviating from the experimental ones due to the presence of the silver layer in the BSCCO tape, which was not considered in this simulation. This layer acts as a parallel path for the current when the BSCCO layer starts quenching, thus, decreasing the total resistive losses.

The main deviations between the Extended-Norris and simulation results occur around $I_m = I_c$, i.e., for I_c = 150 A, as expected due to the discrete behaviour of the Norris hysteretic losses. Please note that for I_m = 150A, the average value of the self-magnetic flux density is about $B_{av} = 23.5$ mT, which decreases the critical current to $I_c = I_{c0}B_0/(B_0 + B_{av}) \cong$ 150 A and thus, $I_m = I_c$. The Sigmoid model produces very accurate results when compared with the FEA, with the same parameters, and experimental results.

In Fig. 21, the silver layer around the SC layer is added to the FEA simulation and analytical models. It is verified that the analytical and FEA losses for high values of currents resemble the experimental ones. To obtain the analytical results, the

equivalent circuit in Fig. 22 was used with an applied sinusoidal current, I_{app}, and based on the equivalent resistances of the HTS tape in section 2.4 and approximated inductances of the superconducting and silver layers.

Regarding the SC layer, its inner inductance coefficient, L_{HTSi}, is non-linear due to the penetration of current over time. Please note that there is no unique representation of inductances in the frequency domain (assuming sinusoidal currents) when the material is non-linear, as is the case of superconductors. Depending on the method used, such as simple energy, average energy, reluctance, or other, different values of effective induction coefficients can be obtained. This effect is similar when computing effective *BH* curves of iron cores [41]. In this work, it is considered the average value of the magnetic flux density inside the SC layer, in (24), to compute the inner flux through the half layer, $\lambda'_i = aB_{av}$, for each applied current amplitude. From this, and assuming linearity, an effective SC layer inductance coefficient, $\hat{L}_{SCi}$, can be estimated as in (24). When full penetration occurs, F=1, $\hat{L}_{HTSi} = 8 \times 10^{-7}$ H, which is similar in magnitude to the value obtained when using the method presented in [42] ($\hat{L}_{SCi} = 9 \times 10^{-7}$ H). Note that the external induction coefficient of the tape is not included in Fig. 22, because with applied current it does not influence the distribution of the current between the superconducting and silver layers.

$$\lambda'_i = aB_{av} \rightarrow \hat{L}_{SCi} = \frac{2\lambda'_i}{I_m} \tag{28}$$

The estimation of the silver matrix resistance, R_{silver}, and inductance, L_{silver}, can be done using rectangular conductors' theory and the skin effect as shown in (29) to (31) [43]. In (31), ω is the angular frequency and $\rho_{al} = 0.4\times 10^{-8}$ Ωm.

$$R_{silver} = K_R \frac{1}{\sigma_{silver} S}, \quad L_{silver} = K_L \mu_0 \frac{a}{b}, \tag{29}$$

$$K_R = \xi \frac{(\sinh 2\xi + \sin 2\xi)}{(\cosh 2\xi - \cos 2\xi)}, \quad K_L = \frac{3}{2\xi} \frac{(\sinh 2\xi - \sin 2\xi)}{(\cosh 2\xi - \cos 2\xi)} \tag{30}$$

$$\xi = 2a\sqrt{\frac{\omega\mu_0}{2\rho_{al}}} \tag{31}$$

Note that the applied current, I_{app}, now divides into the superconducting layer current, I_m, and the silver layer current, I_{silver}. Due to the dependence of the equivalent resistances on the SC layer current, its solution requires an iterative process. It was found that only 1 or 2 iterations are required for $I_m < I_c$, while 4 to 5 are required when $I_m > I_c$.

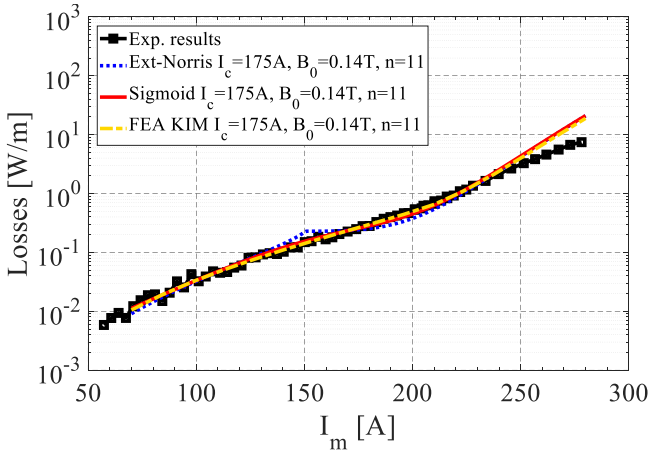

Fig. 20. BSCCO. Comparison between experimental, Extended-Norris, Sigmoid, and FEA results. FEA results consider the Kim model.

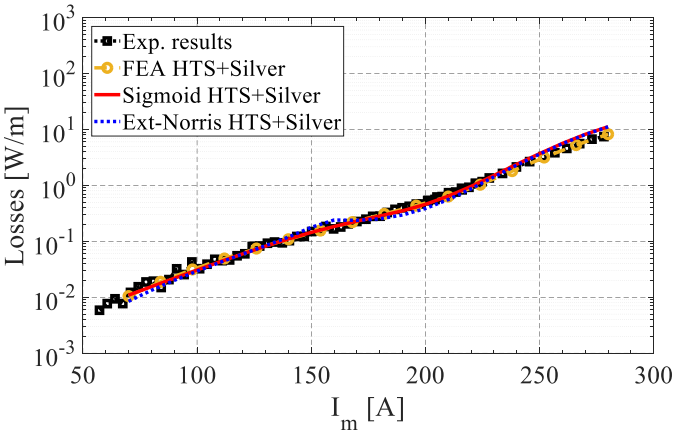

Fig. 21. BSCCO. Comparison between experimental, Extended-Norris, Sigmoid, and FEA results with silver layer.

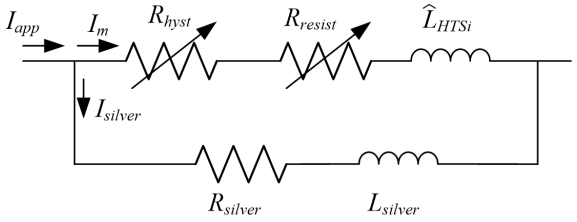

Fig. 22. Equivalent circuit for the inclusion of the silver layer.

4.2.2. ReBCO Tape

The experimental, Extended-Norris, Sigmoid model and FEA results are shown in Fig. 23 and Fig. 24 for the ReBCO tape, without and with the copper layers stabilizers, respectively.

The FEA results are close to experimental results and lay between the Extended-Norris and Sigmoid model results, for the same input parameters of the HTS tape. Regarding experimental results, due to its high n value, the voltage

drastically increased after surpassing I_m=1.2I_c and the experimental measurements were oscillatory. Therefore, the experimental measurements were only recorded until this point.

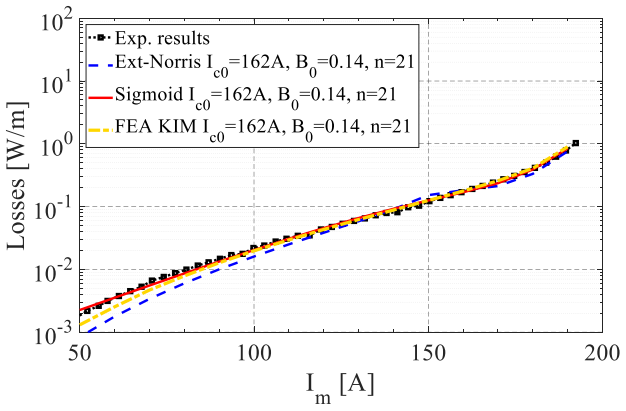

Fig. 23. ReBCO. Comparison between experimental, Extended-Norris, Sigmoid, and FEA results. FEA results consider Bean and Kim models.

The results with the copper stabilizers are also presented in Fig. 24, now for higher values of currents. To apply the analytical model, a similar approach to the BSCCO tape with the silver layer is followed. The equivalent circuit in Fig. 25 is used with an applied sinusoidal current, I_{app}. The equivalent resistances of the HTS tape are defined in section 2.4. The approximated inductances of the superconducting layer and the resistance and inductance of copper stabilizers are estimated using equations (28) to (31) but with the 2nd generator tape geometry and the copper electric resistivity of ρ_{cu} = 0.233× 10^{-8} Ωm. The width and thickness of each copper layer are 4 mm and 20 µm, respectively. Regarding the FEA simulation, the T-A formulation is now used with three layers in parallel. One represents the superconducting layer and two others, surrounding the latter, represent the copper stabilizers, shown in Fig. 26. The relative position and dimensions of each layer were obtained from [44]. To ensure the parallel connection between layers, the global constraint (32) was used.

$$I_{app} = \int J_z d\Omega_{sc} + \int J_z d\Omega_{cu} \qquad (32)$$

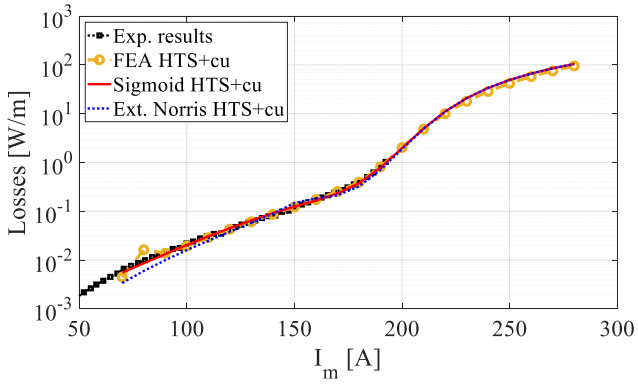

Fig. 24. ReBCO. Comparison between experimental, Extended-Norris, Sigmoid, and FEA results, with copper stabilizers.

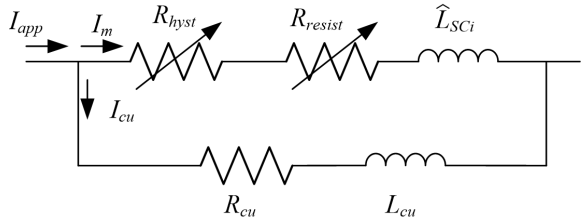

Fig. 25. Equivalent circuit for the inclusion of the copper layer stabilizers.

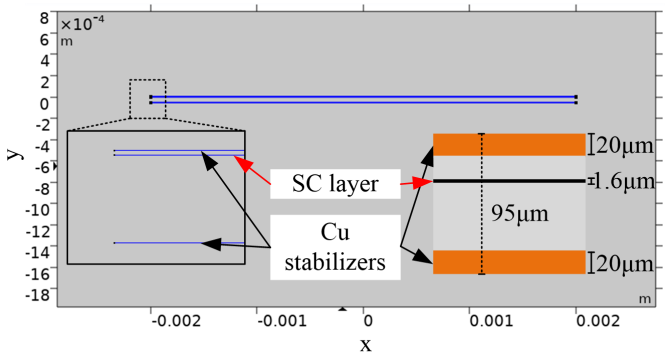

Fig. 26. Geometry used in FEA for the ReBCO with copper stabilizers.

For this tape, the Sigmoid model presented better results. While the Extended-Norris model diverges from the experimental results for lower values of currents, as verified in [17] and [20], the Sigmoid model is capable of presenting good results. Therefore, the proposed analytical models have been verified and can be used as important tools for the identification and simulation of both 1st and 2nd generation HTS tapes.

5. Discussion

The developed analytical models have shown to be capable of accurately predicting the *ac* losses in tested 1st and 2nd generation tapes (BSCCO and ReBCO tapes). The main differences between the Extended-Norris and Sigmoid models are their performance in the transition between the hysteretic and resistive modes, and the physical meaning of their parameters. The Sigmoid model presents a better performance for the whole range of current, including in the transition between the hysteretic and resistive modes, on which the Extended-Norris presents higher deviations. However, its parameters do not provide a physical meaning as in the Extended-Norris model.

Both analytical models allow the development of equivalent circuits, which were used to include the presence of the silver matrix in the BSCCO tape and the copper stabilizers in the ReBCO tape. These equivalent circuit models can be used to estimate the losses of HTS tapes under complex geometries and applications:

i) Where the transition between the SC's hysteretic and resistive modes can occur. This is important because eddy current losses due to external variable magnetic fields are not considered. The main source of *ac* losses is considered to be the transport current losses;

ii) Where the HTS tape current can be decomposed by a set of sinusoidal harmonics. The model was developed for sinusoidal currents with amplitude I_m.
iii) For multiple tapes, for example tape stacks, however, it is required to estimate the distribution of the magnetic field (average magnetic field) at each tape.

6. Conclusions

This work presents two alternative analytical models to characterize the hysteretic and resistive losses of 1st and 2nd generation superconducting tapes, with applied currents: Extended-Norris and Sigmoid models.

The Extended-Norris model is proposed by adding the resistive losses to the Norris model. Compared with finite element and experimental results, this model presents sufficiently accurate results for the overall range of applied current amplitudes. However, it presents one main inaccuracy related to the transition between the hysteretic and resistive states. Between these states, a "knee-point" appears due to the saturation of the analytical Norris hysteretic losses.

To correct this transition, a Sigmoid model is proposed. This model presents a smoother transition between the hysteretic and resistive states, providing results closer to the finite element and experimental results, for both 1st and 2nd generation tapes.

The proposed analytical models were validated with simulation and experimental results. These also allowed the definition of equivalent electric circuits. Due to the presence of a silver matrix in the 1st generation tape and the copper stabilizers in the 2nd generation tape, their equivalent electric circuits were tested with parallel silver and copper layers impedances. Results show that for high current amplitudes, in the resistive state, the applied current starts dividing between the superconducting and silver and copper layers.

The proposed analytical models proved useful, not only for the estimation of hysteretic and resistive losses for 1st and 2nd generation tapes, but also for the identification of their parameters and for the development of equivalent electric circuits. The external *ac* magnetic field's influence and different electric frequencies will be analysed in further works.

Acknowledgments

This work was supported by FCT - Foundation for Science and Technology, I.P., and when applicable co-funded by EU funds, through IDMEC, under LAETA, project UIDB/50022/2020. We also want to acknowledge Prof. Pedro Ramos from Instituto Superior Técnico for allowing us to use the micro-voltmeter Keithley 2000.

References

[1] H. Moon et al, "An introduction to the design and fabrication progress of a megawatt class 2G HTS motor for the ship propulsion application," *Supercond. Sci. Technol*. vol. 29 no. 3, Feb. 2016.

[2] F.F. da Silva; J.F.P. Fernandes; P.J. Costa Branco, "Barriers and Challenges Going from Conventional to Cryogenic Superconducting Propulsion for Hybrid and All-Electric Aircrafts". *Energies*, 14, 6861, 2021.

[3] K. S. Haran, et. al, "High power density superconducting rotating machines—development status and technology roadmap", Superconductor Science and *Technology*, vol. 30, no. 12, 2017.

[4] J. Zhao, X. Zhang, N. Swaminathan and K. S. Haran, "An Overview of High Specific Power Electrical Machines and Drives Technologies for Electrified Aircraft," 2022 *IEEE Energy Conversion Congress and Exposition (ECCE)*, Detroit, MI, USA, pp. 1-8, 2022.

[5] S. Sirimanna, T. Balachandran, N. Salk, J. Xiao, D. Lee and K. Haran, "Electric Propulsors for Zero-Emission Aircraft: Partially superconducting machines," in *IEEE Electrification Magazine*, vol. 10, no. 2, pp. 43-56, June 2022.

[6] M. Biasion, J. F. P. Fernandes, S. Vaschetto, A. Cavagnino and A. Tenconi, "Superconductivity and its Application in the Field of Electrical Machines," *IEEE International Electric Machines & Drives Conference (IEMDC)*, Hartford, CT, USA, 2021, pp. 1-7, 2021.

[7] P. J. Masson, G. V. Brown, D. S. Soban and C. A. Luongo, "HTS machines as enabling technology for all-electric airborne vehicles", *Superconductor Science and Technology*, vol. 20, no. 8, 2007.

[8] P. J. Masson, M. Breschi, P. Tixador and C. A. Luongo, "Design of HTS Axial Flux Motor for Aircraft Propulsion," *IEEE Trans. Appl. Supercond.*, vol. 17 pp. 1533 – 1536, June 2007.

[9] B. Lilia, et. al. "The 2021 room-temperature superconductivity roadmap", *Journal of Physics: Condensed Matter*, vol. 34, no. 18, 2022.

[10] F. Weng, M. Zhang, T. Lan, Y. Wang and W. Yuan, "Fully superconducting machine for electric aircraft propulsion: study of AC loss for HTS stator", *Superconductor Science and Technology*, vol. 33, no. 10, 2020.

[11] J. Zheng, H. Huang, S. Zhang and Z. Deng, "A General Method to Simulate the Electromagnetic Characteristics of HTS Maglev Systems by Finite Element Software," *IEEE Trans. Appl. Supercond*. vol. 28 pp. 1–8, Aug. 2018.

[12] J. F. P. Fernandes and V. M. Machado, "Hybrid A-EHS Method for Fast Computation in Superconducting Bulks," in *IEEE Transactions on Applied Superconductivity*, vol. 32, no. 5, pp. 1-11, Aug. 2022.

[13] B. Shen, F. Grilli and T. Coombs, "Review of the AC loss computation for HTS using H formulation," *Supercond. Sci. Technol*. vol. 33 no. 3, Feb. 2020.

[14] W. T. Norris. "Calculation of hysteresis losses in hard superconductors carrying ac: isolated conductors and edges of thin sheets". *Journal of Physics D: Applied Physics*, vol. 3, no. 4, 1970.

[15] E. H. Brandt, M. V. Indenbom and A. Forkl, "Type-II Superconducting Strip in Perpendicular Magnetic Field", *Europhysics Letters*, vol. 22, no. 9, 1993.

[16] O. Tsukamoto, "AC losses in a type II superconductor strip with inhomogeneous critical current distribution", *Superconductor Science and Technology*, Vol. 18, no 5, 2005.

[17] A. F. Zhao et al., "AC Loss Characteristics of HTS Wires Carrying Currents With Different Waveforms," in *IEEE Transactions on Applied Superconductivity*, vol. 26, no. 4, pp. 1-5, June 2016.

[18] H. Zhang; Z. Wen; F. Grilli; K. Gyftakis; M. Mueller. "Alternating Current Loss of Superconductors Applied to Superconducting Electrical Machines". *Energies*, 14, 2234, 2021.

[19] F. Grilli, R. Brambilla and L. Martini, "Modeling High-Temperature Superconducting Tapes by Means of Edge Finite Elements," in IEEE *Transactions on Applied Superconductivity*, vol. 17, no. 2, pp. 3155-3158, June 2007.

[20] S. Stavrev, F. Grilli, B. Dutoit and S. P. Ashworth, "Comparison of the AC losses of BSCCO and YBCO conductors by means of numerical analysis", *Superconductor Science and Technology*, vol. 18, no. 10, 2005.

[21] A. Sadeghi, S. M. Seyyedbarzegar, M. Yazdani-Asrami, "Transient analysis of a 22.9 kV/2 kA HTS cable under short circuit using equivalent circuit model considering different fault parameters", *Physica C: Superconductivity and its Applications*, VOL. 589, 2021.

[22] M. Yazdani-Asrami, S. Seyyedbarzegar, A. Sadeghi, W. T B de Sousa and D. Kottonau, "High temperature superconducting cables and their performance against short circuit faults: current development, challenges, solutions, and future trends", *Superconductor Science and Technology*, vol. 35, no. 8, 2022.

[23] S. S. Fetisov, V. V. Zubko, S. Y. Zanegin, A. A. Nosov and V. S. Vysotsky, "Numerical Simulation and Cold Test of a Compact 2G HTS Power Cable," in *IEEE Transactions on Applied Superconductivity*, vol. 28, no. 4, pp. 1-5, June 2018.

[24] G. Rashid and M. H. Ali, "Transient Stability Enhancement of Doubly Fed Induction Machine-Based Wind Generator by Bridge-Type Fault Current Limiter," in *IEEE Transactions on Energy Conversion*, vol. 30, no. 3, pp. 939-947, Sept. 2015, doi: 10.1109/TEC.2015.2400220.

[25] P.J. Costa Branco, M.E. Almeida, J.A. Dente, "Proposal for an RMS thermoelectric model for a resistive-type superconducting fault current limiter (SFCL)". Electric Power Systems Research, vol. 80, no. 10, pp. 1229-1239, 2021.

[26] B. Shen, Y. Chen, C. Li, S. Wang, X. Chen, "Superconducting fault current limiter (SFCL): Experiment and the simulation from finite-element method (FEM) to power/energy system software", *Energy*, vol. 234, 121251, 2021.

[27] F. Zheng, C. Deng, L. Chen, S. Li, Y. Liu and Y. Liao, "Transient Performance Improvement of Microgrid by a Resistive Superconducting Fault Current Limiter," in *IEEE Transactions on Applied Superconductivity*, vol. 25, no. 3, pp. 1-5, June 2015.

[28] F. J. M. Dias, G. G. Sotelo and R. d. A. Júnior, "Performance Comparison of Superconducting Machines With Induction Motors," in *IEEE Transactions on Applied Superconductivity*, vol. 32, no. 7, pp. 1-5, Oct. 2022.

[29] T. Nakamura et al., "Experimental and Theoretical Study on Power Generation Characteristics of 1 kW Class Fully High Temperature Superconducting Induction/Synchronous Generator Using a Stator Winding With a Bending Diameter of 20 mm," in *IEEE Transactions on Applied Superconductivity*, vol. 32, no. 6, pp. 1-5, Sept. 2022.

[30] X. Li, L. Ren, S. Guo, Y. Xu, J. Shi, Y. Tang and J. Li, "A novel AC loss measurement method for HTS coils based on parameter identification", *Superconductor Science and Technology*, vol. 35, no. 6, 2022.

[31] E. Pardo, J. Šouc and J. Kováč, "AC loss in ReBCO pancake coils and stacks of them: modelling and measurement", *Superconductor Science and Technology*, VOL. 25, NO. 3, 2012.

[32] S. Zanegin, N. Ivanov, V. Zubko, K. Kovalev, I. Shishov, D. Shishov, V. Podguzov. "Measurements and Analysis of AC Losses in HTS Windings of Electrical Machine for Different Operation Modes", *Applied Sciences*. 2021; VOL. 11, NO. 6.

[33] C. P. Bean "Magnetization of hard superconductors", Phys. Rev. Lett. 8 250–3, 1962.

[34] R. W. Barnard, K. Pearce, L. Schovanec, "Inequalities for the Perimeter of an Ellipse", *Journal of Mathematical Analysis and Applications*, vol. 260, no. 2, pp. 295-306, 2001.

[35] S. Wimbush, N. Strickland, A. Pantoja. "A high-temperature superconducting (HTS) wire critical current database". figshare. Collection. 2016. https://doi.org/10.6084/m9.figshare.c.2861821.v18.

[36] K. Kails, H. Zhang, P. Machura, M. Mueller and Q. Li, "Dynamic loss of HTS field windings in rotating electric machines", *Superconductor Science and Technology*, VOL. 33, NO. 4, 2020.

[37] P. Li, L. Ye, J. Jiang and T. Shen, "RRR and thermal conductivity of Ag and Ag-0.2 wt.%Mg alloy in Ag/Bi-2212 wires", *IOP Conference Series: Materials Science and Engineering*, vol. 102, *Advances in Cryogenic Engineering - Materials: Proceedings of the International Cryogenic Materials Conference (ICMC) 2015* 28 June to 2 July 2015, Tucson, AZ, USA.

[38] J. Yoo, H. Chung, J. Ko and H. Kim, "Long-length processing of BSCCO-2223 tapes made by using Ag alloys sheath," in IEEE *Transactions on Applied Superconductivity*, vol. 7, no. 2, pp. 1837-1840, June 1997.

[39] F. Sass et al.,"H−formulation for simulating levitation forces acting on HTS bulks and stacks of 2G coated conductors," *Supercond. Sci. Technol.* vol. 28 no. 12, Nov. 2015.

[40] T. Benkel et al., "T–A-Formulation to Model Electrical Machines With HTS Coated Conductor Coils," in IEEE Transactions on Applied Superconductivity, vol. 30, no. 6, pp. 1-7, Sept. 2020.

[41] P. P. C. Bhagubai and J. F. P. Fernandes, "Multi-Objective Optimization of Electrical Machine Magnetic Core Using a Vanadium–Cobalt–Iron Alloy," in *IEEE Transactions on Magnetics*, vol. 56, no. 2, pp. 1-9, Feb. 2020.

[42] M. Sjostrom, B. Dutoit and J. Duron, "Equivalent circuit model for superconductors," in *IEEE Transactions on Applied Superconductivity*, vol. 13, no. 2, pp. 1890-1893, June 2003.

[43] I. Boldea, S.A. Nasar. "The Induction Machine Handbook" (1st ed.). CRC Press. 2001.

[44] SuperPower-Furukawa 2023 Superpower 2G HTS coated, conductors (available at: https://www.superpower-inc.com/specification.aspx)

